Wet-Chemical Noncovalent Functionalization of CVD Graphene: Molecular Doping and Its Effect on Electrolyte-Gated Graphene Field-Effect Transistor Characteristics

Mbaye Dieng, Mohamed Bensifia, Jérôme Borme, Ileana Florea, Catarina Abreu, Charafeddine Jama, Céline Léonard, Pedro Alpuim, Didier Pribat, Abderrahim Yassar, et al.

Wet-chemical non-covalent functionalization of CVD-graphene: molecular doping and its effect on electrolyte-gated graphene field-effect transistor characteristics

Mbaye Dieng[1,2], Mohamed Bensifia[3], Jérôme Borme[4], Ileana Florea[2], Catarina M. Abreu[4], Charafeddine Jama[5], Celine Leonard[3], Pedro Alpuim[4, 6], Didier Pribat[2], Abderrahim Yassar[2], Fatima Z. Bouanis*[1,2]

[1]*COSYS-LISIS, Univ Gustave Eiffel, IFSTTAR, F-77454 Marne-la-Vallée, France*

[2]*Laboratory of Physics of Interfaces and Thin Films, UMR 7647 CNRS/ Ecole Polytechnique, IPParis, 91128 Palaiseau-France.*

[3]*MSME, Univ Gustave Eiffel, CNRS UMR 8208, Univ Paris Est Creteil, F-77454 Marne-la-Vallée, France*

[4] *INL - International Iberian Nanotechnology Laboratory, 4715-330 Braga, Portugal*

[5]*Univ. Lille, CNRS, INRAE, Centrale Lille, UMR 8207 - UMET - Unité Matériaux et Transformations, F-59000 Lille, France*

[6] *Department of Physics, University of Minho, 4710-057 Braga, Portugal*

Corresponding author

Univ Gustave Eiffel, IFSTTAR, F-77454 Marne-la-Vallée, France

Tel: +33 (0) 1 69 33 43 85, E-mail address: fatima.bouanis@ifsttar.fr (Fatima Zahra Bouanis)

Abstract:

Graphene sheets (mono- and multi-layers) were synthesized by chemical vapor deposition and functionalized with various aromatic molecules such as Fe-/Co-porphyrin and Fe-phthalocyanine through π-π interactions. The resulting nano-hybrid materials were characterized by Raman spectroscopy (RS), X-ray photoelectron spectroscopy (XPS), atomic force microscopy (AFM), scanning electron microscopy (SEM), and high-angle annular dark-field scanning transmission electron microscopy (STEM-HAADF) techniques. The presence

of physi-adsorbed molecules (Fe-/Co-porphyrin and Fe-phthalocyanine) on the graphene sheet surface is evidenced by spectroscopic and microscopic analysis, which confirm that these molecules are immobilized through electrostatic and π-π interactions. RS confirmed the n- or p-type doping of graphene, according to the chemical nature of those physi-adsorbed molecules. The electrical characteristics of electrolyte-gated graphene field-effect transistors (GFETs) based on nano-hybrid materials were subsequently evaluated and demonstrated a charge transfer between the physi-adsorbed molecules and the graphene. All these results suggest that the electronic structure of graphene can be tailored by doping with aromatic molecules. Density Functional Theory (DFT) calculations were performed to confirm these observations.

Keywords: Graphene; Porphyrin; Phthalocyanine; Non-covalent Functionalization; electrolyte-gated GFET.

1. Introduction

Since the isolation of mono- and few-layers graphene, an atomically thin two-dimensional carbonaceous honeycomb, it has become one of the most investigated materials, thanks to its exceptional electrical, mechanical, and chemical properties [1-3]. In particular, the high surface-to-volume ratio, excellent carrier mobility, high thermal conductivity, excellent chemical properties, and unique optical characteristics of graphene make it suitable for a wide range of applications [4]. However, graphene is a semimetal with zero bandgap,which restricts its use in many applications that exploit a semiconducting behavior, such as gas sensing, where an appropriate bandgap is requisite.

Non-covalent doping has recently emerged as an elegant way to increase graphene's carrier density and adjust its work function [5-7]. Considerable efforts have been made to modify the graphene surface, with organic or inorganic molecules, in order to fabricate graphene nano-hybrid materials for nano-electronic and sensing applications. This effort is

motivated by the fact that these hybrid materials combine the unique electrical, optical and chemical properties of their components and offer the potential to generate synergies from the peculiar properties of each of those components.

Chemical modification of graphene sheets with small organic molecules represents a viable approach for tailoring electronic properties such as band gap opening. Both covalent and non-covalent chemical methods have been investigated for this purpose [8-12]. The latter was proven to be a more versatile approach to tune the electronic properties of two-dimensional layered material, via charge transfer doping, defect engineering, and device performance improvement, etc., since it preserves its π-extended conjugated sp^2 network [13].

There is a plethora of aromatic and non-aromatic molecules including, alkyl-amines [14], 7,7,8,8,-tetracyanoquinodimethane [15], pentacene, and phthalocyanine [16], capable of inducing controllable molecular doping of graphene. The doping process is accompanied by a change in the electronic properties providing thus characteristic signatures, which are essential for sensing applications. Among these molecules, macrocyclic metal complexes with planar structures are excellent candidates for this purpose since they can be easily chemically anchored or physi-adsorbed on the graphene surface through π−π interactions. Furthermore, combining graphene with planar macrocyclic metal complexes provides new functionalities, thanks to the synergy from both components. Consequently, several studies have shown that porphyrins (Por) or phthalocyanines (Phc) graphene hybrid photodetectors exhibit enhanced photo- and chemical responses compared to the pristine graphene [17-20].

Regarding the molecular doping and its effect on the electronic properties, non-covalent functionalization of graphene sheets by Por has shown a clear evidence of doping by charge transfer processes, as well as graphene's work function modulation. Using a statistical analysis of scanning tunneling spectroscopy measurements, Arramel *et al.* [21] demonstrated that the non-covalent interaction of metallic porphyrins with Chemical Vapor Deposition

(CVD)-graphene sheets could cause a bandgap opening that could be tuned, by changing the central metal of the porphyrin. Gajarushi *et al.* [22] investigated the electronic properties of graphene non-covalently functionalized with porphyrin and its metalled form, zinc-porphyrin. The non-covalent functionalization of graphene using porphyrin molecules showed a positive shift of the transfer curve and Dirac point in graphene field-effect transistors (GFETs), enhanced hole current, and reduced electron current. When implemented in chemiresistive sensor, many Por molecules show strong dipoles once bound to an analyte and relatively weak dipoles in their unbound states. These strong dipole interactions alter the carrier concentration in the underlying graphene and ultimately modulate the sensor conductivity based on analyte concentration [23]. Pyo *et al.* [24] reported a highly sensitive, flexible and transparent UV detection and vapor toluene sensing chemiresistor based on CVD graphene functionalized with Por via one-step evaporation. Co porphyrin was deposited on the graphene by thermal evaporation. To investigate the influence of Co porphyrin functionalization on the electronic properties of graphene, they fabricated a field-effect transistor. The electrical measurements revealed that sensors were n-doped, and their resistance decreased upon exposure to toluene. Swager and co-workers [23] fabricated a highly sensitive ammonia gas chemiresistor based on Co porphyrin functionalized graphene CVD. The gas chemiresistor device was fabricated by drop-casting a porphyrin solution on a CVD-graphene sensor array. Porphyrin-functionalized graphene exhibited enhanced ammonia sensitivity compared to pristine graphene.

In most cases, when organic molecules are used to functionalize the graphene surface, they are deposited on graphene sheets by vapor-phase and form island structures. However, to realize low-cost fabrication processes for organic-graphene hybrid electronics, physical vapor deposition methods are not compatible with low-cost products (plastic substrates). Wet-chemical non-covalent functionalization of graphene with small molecules offers a simple and

economical way to produce large quantities of hybrid materials with many functionalities, using low-cost equipment. Moreover, chemically functionalized 2D materials possess a high potential for developing novel functional devices for new applications. Although the molecular functionalization of graphene with monolayers that can serve as dopants is well established, new advanced characterization techniques that can be used for nano-hybrid structured materials are not extensively developed.

This work combines several experimental characterization methods with theoretical calculations to develop a deep understanding of the interaction and the influence of Por and Phc on the electronic properties of CVD graphene sheets. Metalloporphyrins (MPo) and methalophthalocyanines (MPc) molecules were chosen because their aromatic backbone promotes non-covalent bonding with the graphene plane, and they have strong dipoles when interacting with specific gas analytes, making them good candidates for the fabrication of selective graphene gas-detecting materials. The functionalization with Fe-porphyrin, Co-porphyrin, and Fe-phthalocyanine was carried out using a drop-casting method. The graphene sheets were synthesized by CVD on high purity copper foils [25]. These metallo-aromatic molecules form a stable adsorbed layer attached to the surface of graphene. A partial electron transfer between graphene and molecular adsorbed layer results in p-type or n-type doping of the graphene depending on the type of the molecules and the metal of the complexes. These results are confirmed by Raman spectroscopy, energy dispersive spectroscopy, X-ray photoelectron spectroscopy, atomic force microscopy (AFM), scanning electron microscopy, and transmission electron microscopy.

The charge transport studies were performed using electrolyte-gated GFET devices in ambient air to probe the change in the electrical properties of Por/Phc graphene nanohybrid materials and Por/Phc and to confirm graphene's doping effect. A theoretical approach is

developed to evaluate the charge transfer between the metal-centered molecules and graphene.

2. Material and methods

2.1. Synthesis of graphene

Single-layer graphene was synthesized by thermal CVD on high purity copper foils (Goodfellow Cu000410: 99,99+% purity, 0.025 mm thick), according to the process published previously [25]. Briefly, the copper foil is cut into 10 cm × 10 cm parts and fit into a graphite confinement box which isolates the substrate from sources of contamination. The substrate is introduced into a three-zone quartz tube furnace (EasyTube ET3000, CVD Corp.) and first annealed at 1020 °C for 20 min in a hydrogen atmosphere (300 sccm, 0.5 Torr). The gaseous carbon source is a mixture of methane and hydrogen (H_2:CH_4 6:1, 0.5 torr) that flows into the furnace for 30 min while keeping the temperature at 1020 °C. The transfer is performed by plasma etching the graphene from one of the sides of the copper sheet and spin-coating a poly(methyl methacrylate) (PMMA) support layer on the graphene on the other side (1600 RPM dried vertically overnight at 20 °C). Then the Cu foil is dissolved in 0.48 M $FeCl_3$ at 35 °C for 30 min, followed by rinsing in 3 cycles of chemical baths (per cycle: 5min in water; 30min in 2% HCl, v/v) and manual transfer onto a 200 mm oxidized p-type silicon wafer. The PMMA layer is finally dissolved (sample dipped in acetone overnight, followed by a two-hours, 300 °C bake).

2.2. Functionalization of graphene sheets

All reagents (5,10,15,20-Tetraphenyl-21H,23H-porphine iron (III) chloride (Fe-Por) (94%), 5,10,15,20-Tetraphenyl-21H,23H-porphine cobalt(II) (Co-Por) (85%) and iron (II) phthalocyanine (Fe-Phc)) (90%), as well as organic solvents (dichloromethane (DCM)) and acetone) were purchased from "Merck". The reagents were used without further purification.

Prior to functionalization, the CVD-graphene samples were intensively cleaned by acetone and isopropanol, followed by drying under N_2, to remove organic impurities like remaining polymer residues adsorbed on the graphene surface or other residues coming from the production, to improve its wetting properties, and to avoid coffee-ring formation. Contact angle measurements were performed to examine the wetting properties of CVD-graphene. Contact angle measurements were conducted with a Fluidican Rheo apparatus at ambient temperature. A dichloromethane droplet of 10 µL was formed at the end of the syringe and carefully deposited onto the CVD-graphene surface. The syringe was withdrawn and the image of static contact angle was taken within 10 secondes of solution deposition by a charge coupled device (CCD) camera. The contact angle was calculated by Origin software. The reported contact angle values are based on 5 repeats.

The functionalization of the graphene was achieved following our previously published procedures [26]. The Por or Phc compounds were dissolved in DCM at a 5.10^{-3} mol/l Fe-Por concentration, a 10^{-4} mol/l Co-Por concentration, or a 5.10^{-4} mol/l Fe-Phc concentration. 10 µl of Por or Phc solution was drop-cast onto the surface of a graphene sheet. Then, the surface was dried for one hour at 100°C gradually. After rinsing several times with acetone to remove the excess of unbound molecules, the functionalized graphene (Fe-Por-graphene, Co-Por-graphene, or Fe-Phc-graphene) was then dried at 40 °C for 5 min.

2.3. Characterization methods

Different techniques were used to characterize the structure, microstructure, and composition of nano-hybrid materials. The efficiency of the physi-adsorption process was first evaluated by Raman spectroscopy. The morphology of the nano-hybrid materials was microscopically analyzed using Atomic Force Microscopy (AFM), Scanning Electron Microscopy (SEM) and Transmission Electron Microscopy (TEM). The chemical properties

and elemental composition of nano-hybrid materials were characterized by Energy Dispersive Spectroscopy (EDS) and X-ray photoelectron spectroscopy (XPS). The transport studies were performed using electrolyte-gated GFET devices in ambient air. The theoretical density functional theory calculations (DFT) (open-shell) were carried out using the CRYSTAL17 code.

2.3.1. Raman spectroscopy. Raman spectra were recorded using a high-resolution confocal Raman microscope (Labram HR800; HORIBA Jobin Yvon France) through a 100× microscope objective (NA=1) to demonstrate the presence of porphyrin and phthalocyanine after functionalization. Micro-Raman mapping was performed in high-resolution mode, using laser excitation of λ=532 nm with 20s acquisition time and two accumulations per spectrum. The number of gratings in the Raman spectrometer was 600 grooves per mm. Raman mapping was performed on 5 µm × 5 µm areas with a step size of 0.2 µm.

2.3.2. Atomic Force Microscopy (AFM). Atomic Force Microscope (AFM) images were acquired using a Dimension icon with Scan A system instrument.

2.3.3. Scanning Electron Microscopy. Scanning Electron Microscopy (SEM) observations were carried out using HITACHI S 4800 electron microscope. Further, to investigate the chemical state of the functionalized graphene, energy dispersive spectroscopy (EDS) analyses (Thermo Ultra Dry) were performed.

2.3.4. High Resolution-Transmission Electron Microscopy and Scanning Transmission Electron Microscopy. The High Resolution-Transmission Electron Microscopy **(**HR-TEM) analyses were performed using a Thermo Fisher Titan-Themis electron microscope operating at 80 and 300kV. For the graphene characterization (before and after functionalization), an operating voltage of 80 kV was used to avoid any beam damage. Before the TEM observations, a preliminary step was mandatory, consisting of transferring the graphene from the substrate surface onto Cu-mesh TEM grids. This has been done using a polymethyl

methacrylate (PMMA) transfer method [27]. The PMMA was spin-coated onto the Si/SiO_2-graphene at 3000 rpm for 40 s, followed by drying at 100°C for 5min. Then, the Si/SiO_2 was etched in NaOH (1mol/l) for one hour. The graphene/PMMA was removed and placed into deionized (DI) water baths. After rinsing several times with DI water, the PMMA/graphene assembly was carefully deposited onto the TEM grid. Finally, the TEM grids were dried at 100°C for 24h, and then the PMMA was dissolved in acetone. The molecules (Por or Phc) were deposited by a drop-casting of a 10µL drop of a solution (Por or Phc) in DCM directly on top of the graphene surface, followed by a thorough acetone washing process of non-grafted molecules. In order to probe the presence of Por element components (Fe or Co) or Phc (Fe) chemical state, energy dispersive spectroscopy (EDS) analyses have been performed on a 200kV Titan-Themis TEM/STEM electron microscope equipped with a Cs probe corrector and a Chemistem Super-X detector. These two accessories allow chemical mapping of the light and heavy elements with a spatial resolution in the picometer range. To avoid sample damage during the Scanning Transmission Electron Microscopy (STEM)-HAADF chemical analysis, the acquisition conditions have been slightly modified to use a very low beam current.

2.3.5. X-ray photoelectron spectroscopy

X-ray photoelectron spectroscopy (XPS) measures were performed using an XPS KRATOS, analytical AXIS UltraDLD spectrometer Thermo Scientific KAlpha XPS system (UK). The monochromatized Aluminium-Kα X-ray source ($h\upsilon$ = 1486.6 eV) was set-up via an electromagnetic lens mode and in a constant analyser energy mode (CAE = 150 eV for survey spectra and CAE = 30 eV for high resolution spectra). The binding energy scale was initially calibrated using the Ag 3d5/2 (368.2 eV), Cu 2p3/2 (932.7 eV) and Au 4f7/2 (84 eV) peak positions. In addition, the C 1 s hydrocarbon (285.0 eV) binding energy (BE) was used as an internal reference for calibration. Simulation and quantification of the experimental

peaks were performed using the Casa XPS software. Moreover, quantification took into account a nonlinear Shirley background subtraction [28].

2.3.6. Charge transport studies.

The transistor architecture used is planar, with a receded gate included within a 2.8 mm of diameter, with an effective exposed area of 3.03×10^6 μm^2, a channel width of 75 μm, and a channel length of 25 μm. A detailed account of the fabrication procedure for GFETs, following the method of a transfer assisted by a metallic sacrificial layer, is described elsewhere [29] and briefly given below:

GFET fabrication: A back-gate access is first prepared by lithography and reactive ion etching on a 200 mm silicon wafer (p-doped, Si-mat) covered with 100 nm of thermal oxide. A thin metal film (Cr 3 nm / Au 30 nm / Al_2O_3 20 nm) is deposited and patterned into contacts by optical lithography and ion milling performed at 40° from normal incidence. A sacrificial layer (TiWN 5 nm / Al 100 nm / TiWN 15 nm) is deposited, by lift-off, on the wafer excepted the place of the graphene channel. Graphene is transferred by the wet technique explained above and patterned by ICP (1200 W, O_2 100 sccm, 0.03 mbar, 30 s). The sacrificial layer is removed by wet etch steps (H_2O_2 30% 150 s, AZ400K 1:4 240 s, H_2O_2 30% 50 s). A stopping layer consisting of Cu 10 nm / AlSiCu 30 nm / TiWN 15 nm is sputtered onto the graphene channel and patterned by lift-off into gate electrode and contact pads. A silicon oxynitride passivation is then grown by PECVD onto the wafer. CVD single-layer graphene is transferred onto the wafer in nine transfer steps of individual graphene patches, each with dimensions approximately 4 cm x 4 cm, continuously covering the wafer processing area, spanning approximately 12 cm x 12 cm. Then, the transistors are lithographically patterned and etched in reactive ion etching down to the stopping layer, which is then removed by wet etch, finalizing the device.

GFET to probe doping of graphene: Electrolyte-gated GFET was used to probe the doping of graphene. In such a device structure, a droplet of deionized water was used as an electrolyte. The electrical characteristics of electrolyte-gated GFETs were measured using a semiconductor parametric analyzer Keithley 4200-SCS under ambient conditions by applying a source-drain voltage (V_{DS} = 1mV) and measuring the source-drain current (I_{DS}) as a function of the source-gate voltage (V_{GS}).

GFET Functionalization: The functionalization was carried out by drop-casting 10 µl of a solution of molecules (Fe-Por or Co-Por or Fe-Phc in DCM) on the GFETs surface followed by a drying step (1h at 40°C). The device was then thoroughly rinsed several times with acetone to remove unbound molecules.

3. Results and discussion

To evaluate the homogeneity of the wet-chemical functionalization process, we performed the contact angle measurements to examine the wetting properties of CVD-graphene before functionalization (Figure S1). When 10 µL dichloromethane droplet is dropped on the surface of as-produced CVD-graphene, the dichloromethane droplet immediately spread on the surface with dichloromethane contact angles of 25.24 ± 0.42°. This result was reproducible and consistent for all samples, with a uniform response across samples suggesting a homogeneous wet-chemical deposition of the molecules.

Raman spectroscopy is a powerful non-destructive tool to characterize carbonaceous materials, particularly for distinguishing ordered and disordered crystal structures of carbon. Moreover, it has been widely used to reveal the number of stacked graphene layers and distinguish the n- and p-type doped graphene resulting from band shifts [7]. Interaction between graphene and Fe-Por-graphene, Co-Por-graphene, and Fe-Phc-graphene in the nanohybrid materials was first studied by Raman spectroscopy. Figure 1 shows the Raman spectra of graphene, Fe-Por-graphene, Co-Por-graphene, and Fe-Phc-graphene. All Raman

spectra were recorded at an excitation wavelength of 532 nm under ambient conditions. The Raman spectra display three bands; a weak D band at ~1350 cm^{-1} corresponding to defect-induced zone boundary phonons, a strong G band at ~1585 cm^{-1} characteristic of in-plane optical mode of sp2-hybridized carbon, and a broad 2D band at ca. ~2695 cm^{-1} attributed to two-phonon double resonance process [30, 31]. The characterization at different areas at the edge and the central region of several samples shows that the graphene film contains a mixture of monolayer and few-layer graphene flakes (see Figure 1(a) and Figure 1(b)). By comparing pristine (unfunctionalized) and functionalized graphene, new peaks appeared in the latter, between 1050 and 3000 cm^{-1}, which probably reveals the presence of physi-adsorbed molecules. The surface of silicon substrates was functionalized with Fe-porphyrin, Co-porphyrin, and Fe-phthalocyanine following the same process and then analyzed with Raman spectroscopy (see Figure S2 in the supporting information (SI)) to confirm this hypothesis. The resulting mapping shows several peaks between 1000-3000 cm^{-1} that are identical or close to those previously observed on fonctionalized graphene. Figure 1 shows that these bands are characteristics of the physi-adsorbed molecules (see Figure S2). Moreover, a decrease of I_{2D}/I_G (the 2D band intensity divided by G band intensity) was also observed. Indeed, the I_{2D}/I_G ratios are 1.694 ± 0.005 for graphene, 0.892 ± 0.025 for Co-Por-Graphene, 0.765 ± 0.005 for Fe-Phc-Graphene, and 0.623 ± 0.018 for Fe-Por-Graphene. These measurements were obtained from 45 spectra taken on different zones on each sample. All these confirm that these aromatic molecules cause an apparent decrease in I_{2D}/I_G, which can be ascribed to graphene doping [7, 32]. The above results can be explained by the fact that all these molecules possess a large aromatic system, which helps to form a stable adsorbed layer on the surface of graphene through π-π interactions. As reported in [33], These π-π interactions are favorable for the charge transfer between porphyrins and phthalocyanines and the graphene. Therefore, the ratios of the D to the G band changes only slightly (Fe-Por-

graphene (~ 0.75), Co-Por-graphene (~0.72), Fe-Phc-graphene (~ 0.70) and graphene (~ 0.76)), from 0.7 to 0.76 after functionalization, confirming that the functionalization does not destroy the extended π-conjugation system of the graphene [34]. Furthermore, the Raman data show a single 2D Lorentzian peak (ca. 2700cm^{-1}) before and after functionalization, consistent with an unperturbed π band, indicating that graphene's fundamental structural properties remain intact after its non-covalent chemical functionalization with Fe-porphyrin, Co-porphyrin, and Fe-phthalocyanine [35-36]. In order to evaluate the homogeneity of the functionalization process, different areas at the edge and the central region of samples were analysed and typically showed similar characteristics and signal intensities. This result clearly indicates the presence of adsorbed-molecules on top of graphene at each zone, which confirm that the coffee ring effect is minimized.

The doping of aromatic molecules on graphene decreases the intensity ratio of I_{2D}/I_G and affects the Raman frequencies of pristine graphene. Upon n- or p-type doping, the 2D peak position, Pos (2D), shifts from its initial position to higher wavenumbers. However, the G band position, Pos(G), shifts upwards with the p-type doping and vice-versa shifts downwards with the n-type doping [5, 7]. To obtain quantitative analysis of the doping effect of graphene with aromatic molecules, multiple measurements were carried at different zone on each sample. Therefore, a large number of Raman spectra (5 maps, each one containing 120 spectra) were collected on each sample before and after functionalization. Figure 2 presents Pos (2D) versus Pos (G) for pristine graphene, Fe-Por-graphene, Co-Por-graphene, and Fe-Phc-graphene. As indicated from the statistical results of figure 2, Pos (2D) and Pos (G) are shifted after functionalization by Fe-porphyrin, Co-porphyrin, and Fe-phthalocyanine. Indeed, Pos (G) is upshifted for Fe-Phc-graphene, thus indicating that Fe-Phc have induced p-type doping (decreasing electron concentration) in pristine graphene. On the contrary, Pos (G) is downshifted for Fe-Por-graphene and Co-Por-graphene, which suggests that Fe-Por and

Co-Por molecules cause n-type doping (increasing electron concentration) in the graphene. This frequency shift is compatible with a doping-induced change of the Fermi energy and consistent with a charge transfer between the graphene and aromatic molecules [5, 7, 37]. On one hand the Raman spectroscopy confirms that the Fe-porphyrin, Co-porphyrin, and Fe-phthalocyanines molecules remain at the graphene surface despite intensive washing with acetone. On the other hand, these results demonstrate an effective charge transfer effect from Por and Phc to the graphene while suggesting the non-covalent interaction of these molecules and graphene.

To assess the influence of the concentration, we optimized the process of the functionalization of the graphene by studying the influence of the concentration of the three investigated molecules. The Raman spectra of Fe-Por for each concentration are shown in Figure S3 and Table S1 in SI. A similar effect of the concentration of aromatic molecules on Fermi level shift based on point Dirac shift and Raman spectroscopy, the shifts of G and 2D peaks and the changes in the I_{2D}/I_G ratio, has been reported in a recent study [38]. Only results that lead to a high surface coverage was used to investigate the electrical and the morphological studies.

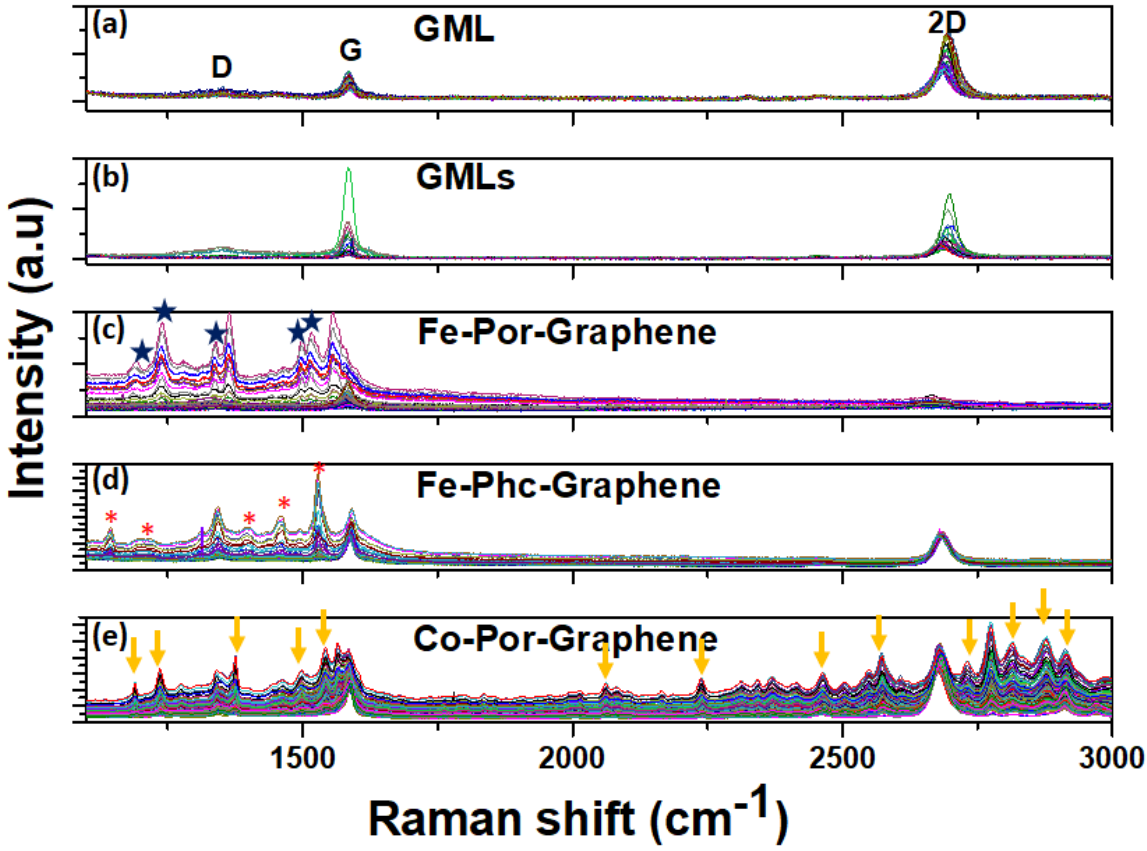

Figure 1. Raman spectra of (top to bottom) graphene monolayer, graphene multi-layers, Fe-Por-graphene, Fe-Phc-graphene, and Co-Por-graphene. (λ_{exc}=532 nm).

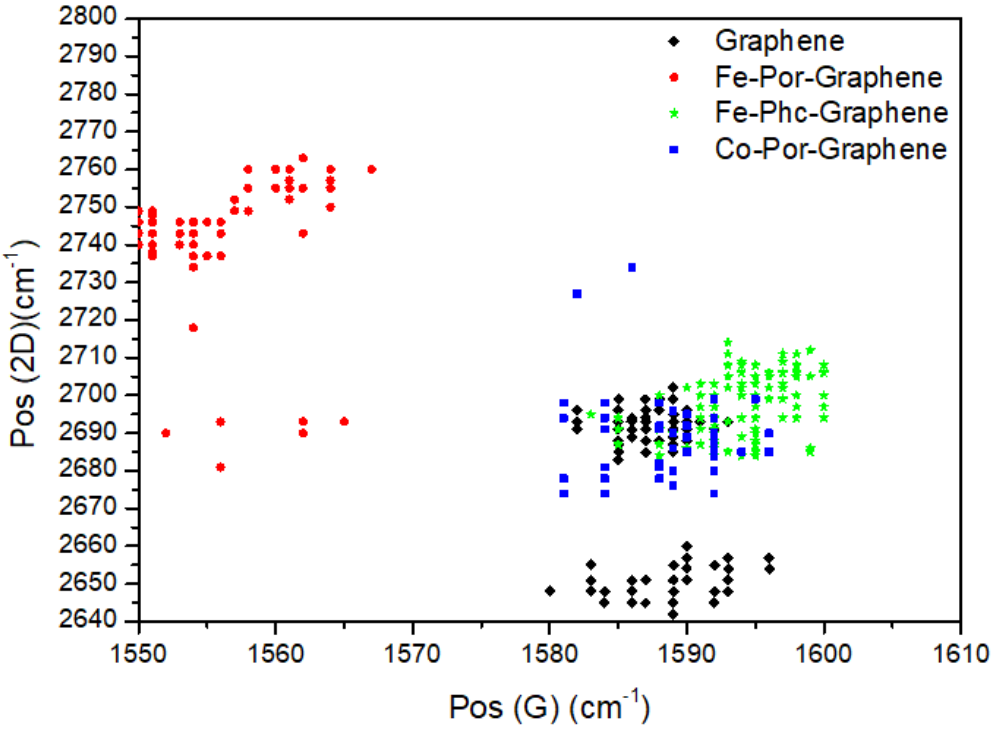

Figure 2. Position of the Raman 2D peak (Pos (2D)) versus position of the Raman G peak (Pos (G)) of graphene before and after functionalization with Fe-Por, Co-Por and Fe-Phc via drop- coating.

To investigate the topography of the functionalized CVD-graphene samples, AFM studies were performed (Figure 3). For bare CVD-graphene (Figure S4), before functionalization, the topography of the surface changes within a small range across the sample surface due to presence of defects, e.g. polymer transfer. After the functionalization AFM analysis showed that the molecules form a spherical like shape (Figure 3). Their height was mostly distributed in the range of 3 to 5 nm, suggesting that the physi-adsorbed molecules consist of few layers of molecules. For each of the investigated molecules AFM topographic images with a line profile are shown in the SI (Figure S5-S9). Different surface morphologies are observed and consist with literature reports. Thus different assembly structures like, two dimensional or one-directional islands have been observed during growth of MPcs on CVD-graphene, and attributed to the domination of either intermolecular interaction and molecule-substrate interactions [39].

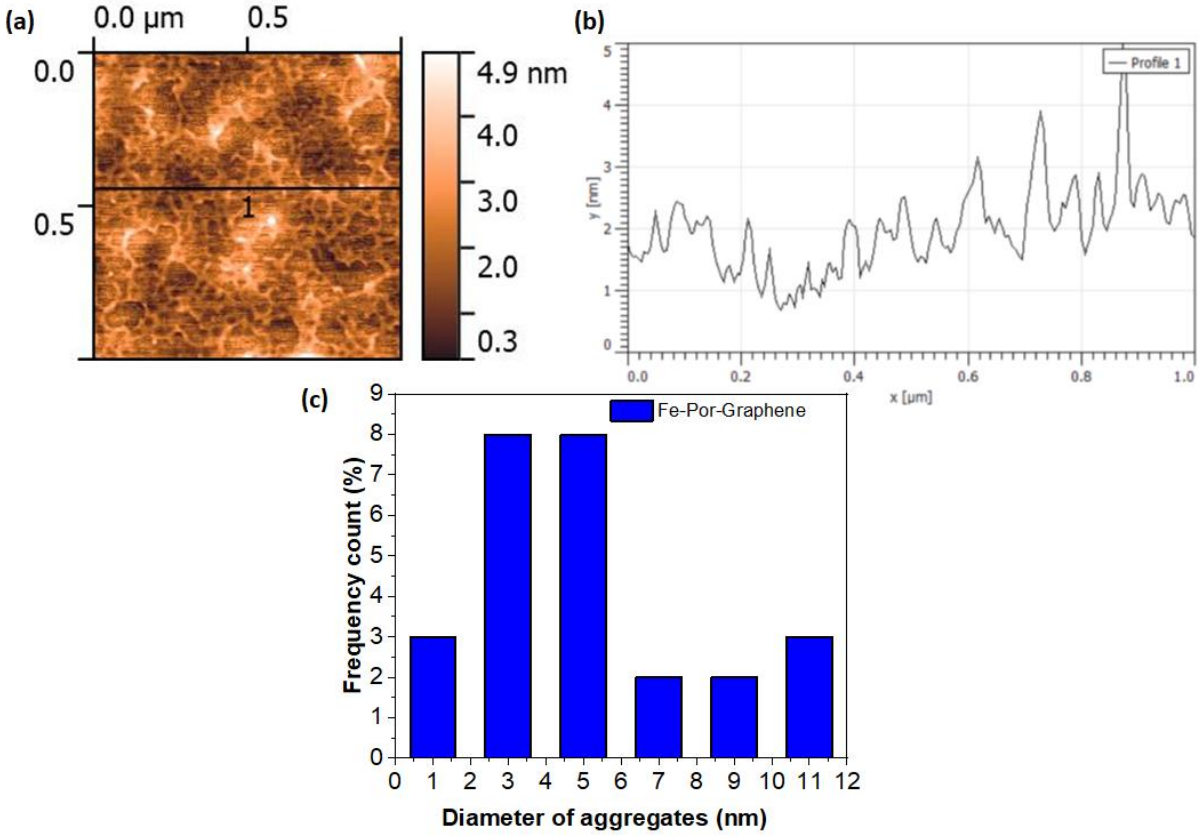

Figure 3. (a) AFM image of Fe-Por islands on CVD graphene. (b) Hight profile of the black line in the image. (c) island size height distribution of Fe-Por aggregates deposited on CVD-graphen.

The existence of the functional molecules on the surface of CVD-graphene was-further investigated by SEM and TEM analysis. SEM analysis was utilized to characterize the microstructure of the graphene and functionalized graphene on silicon substrates. Typical SEM images of graphene and functionalized graphene are displayed in Figure 4. As shown in Fig. 4(a), Fig. 4(c), Fig. 4(e) and Fig. 4(g), functionalized graphene exhibits a layered structure, with a wrinkled surface. The functionalization does not cause significant changes in the graphene flakes structure. Some aggregates with different sizes were observed in some areas on the functionalized surfaces (see Figure S10). To determine their chemical composition, we performed element mapping using the EDS technique, which indicates the presence of Fe and Co elements but in small quantities (Figure 4(d), 4(f), and 4(h)),

suggesting again that the porphyrins and phthalocyanines are physi-adsorbed onto the graphene sheets.

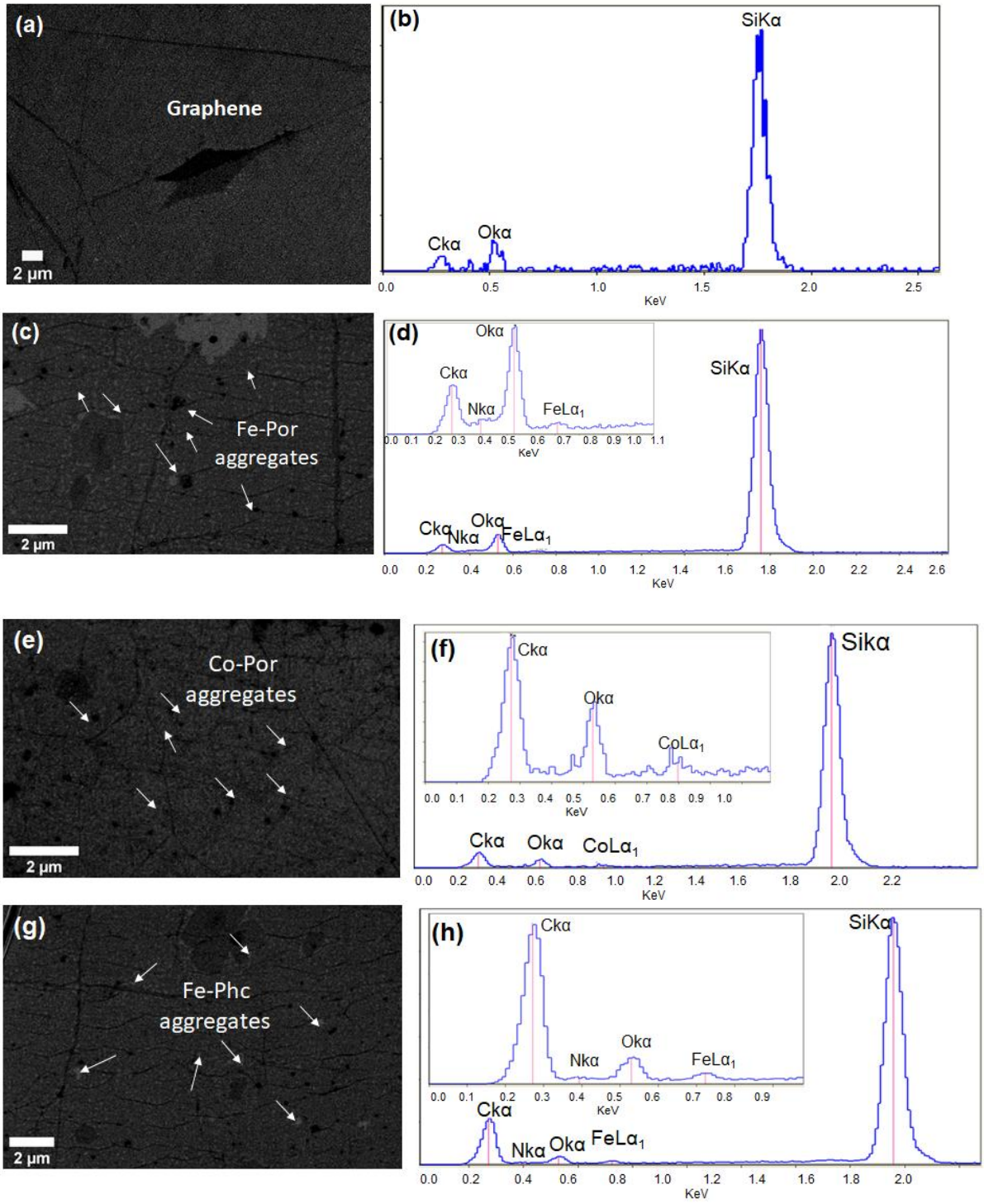

Figure 4. SEM images of graphene (a) and functionalized graphene with Fe-Phc (c), Co-Por (e), and Fe-Por (g). Energy-dispersive X-ray analysis (EDS) spectra of graphene (b) and Fe-Por-graphene (d), Co-Por-graphene (f), and Fe-Phc-graphene (h).

The TEM and STEM analysis further confirmed the formation of the as-prepared nanohybrids. Figure 5(a) displays TEM images of graphene after transfer onto the TEM holey carbon grid. TEM images of graphene layers were obtained for all samples. Furthermore, according to the TEM observations, the graphene flakes appear relatively thin and transparent. More TEM images of pristine graphene are shown in figure S11 in supporting information. The corresponding electron diffraction pattern of the chosen area (the inset of Figure 5(a)) indicates the crystalline structure of the graphene sheet with some amorphous part, which is most probably due to the transfer process where the PMMA polymer has not been completely removed.

Figure 5(b) shows Fe-Por aggregates with different sizes (the areas marked by the yellow circle). Regarding the functionalized graphene, some TEM images of the Fe-Por graphene hybrid structure are shown in Figure 5(c), Figure 5(d), and Figure S12 (SI) showing a relatively large and transparent graphene sheet with the presence of some small aggregates (the area marked with arrow) on the graphene surface. Similar results were also observed for Co-Por-graphene, and Fe-Phc-graphene, respectively (see Figure S13 and S14 in SI).

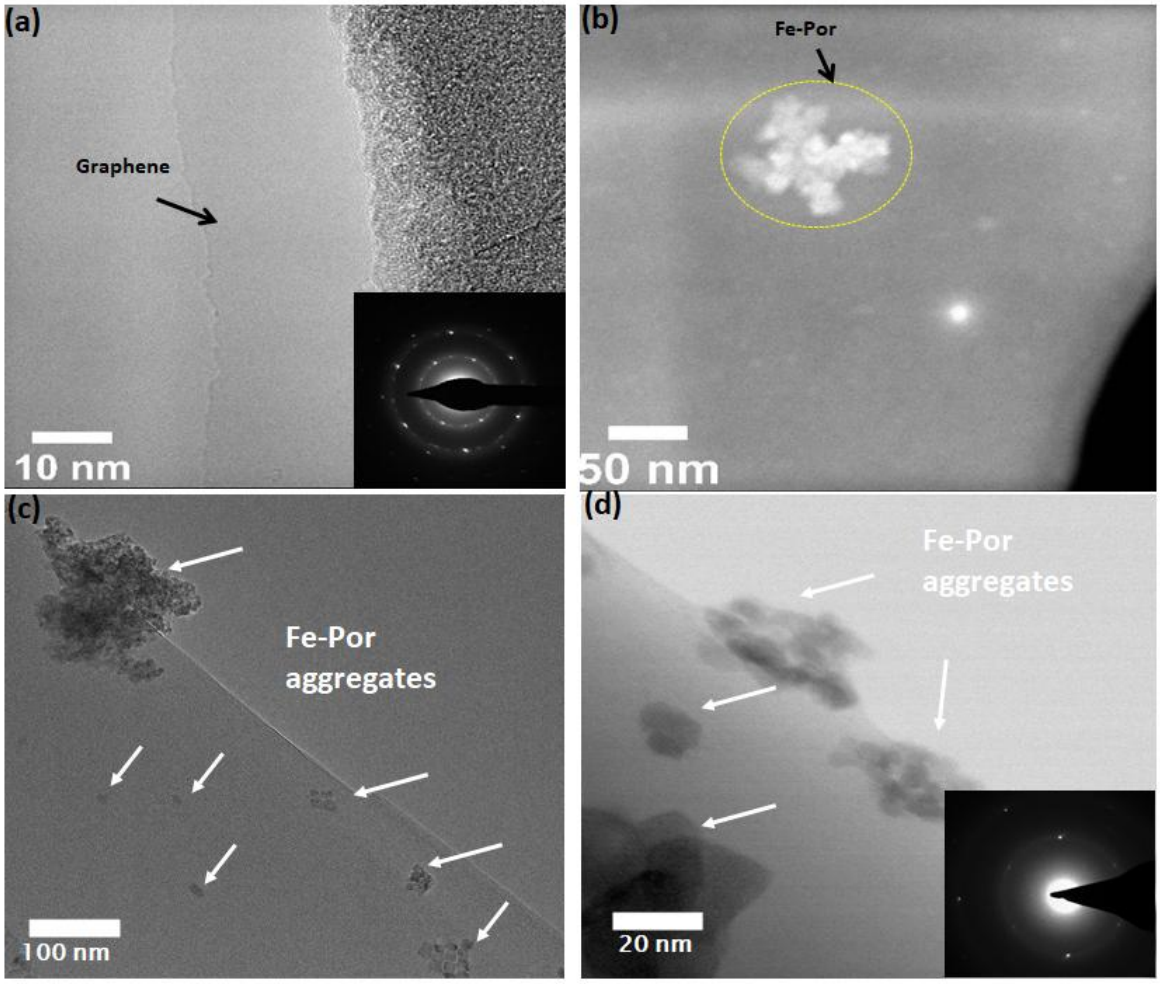

Figure 5. TEM observations of graphene before and after functionalization with Fe-Por. (a) TEM image of a pristine graphene sheet. (b) STEM-HAADF image of Fe-Por. (c-d) HR-TEM image of functionalized graphene with Fe-Por.

To complete the SEM and TEM observations and to get more insight into the non-covalent functionalization of Fe-Por-graphene hybrid structure, chemical analyses using the energy-dispersive X-ray spectroscopy technique in the scanning transmission electron microscopy- high angle annular dark field (STEM-HAADF-EDS) mode of the electron microscope have been performed on different areas of the sample. This type of analysis enables a better identification of the presence of the Fe-Por on the top of the graphene structure. As elements of interest, we have chosen the K edges of Carbon (C) at 0.277 keV, Nitrogen (N) at 0.392 keV, Oxygen (O) at 0.523 keV and Iron (Fe) at 6.408 keV.

Figure 6 displays STEM-EDS line scan analyses recorded on a chosen area on the surface of Fe-Por-graphene. From this Figure, we can identify the elemental signal of Fe and N, suggesting the presence of Fe-Por on the surface of graphene. From the STEM-HAADF image illustrated in figure 6(a), a chemical image where the intensity is directly related to the atomic number, the Fe presence is difficult to identify within the aggregate. However, from the STEM-HAADF EDS line scan spectra recorded along the yellow arrow in the image, the Fe presence in a small amount can be observed. More similar analyses on different areas within the same sample are illustrated in Figure S15 and Figure S16 in SI. Similar results were also obtained for Co-Por-graphene and Fe-Phc-graphene and are presented in Figure S17, S18, S19, and S20 in SI.

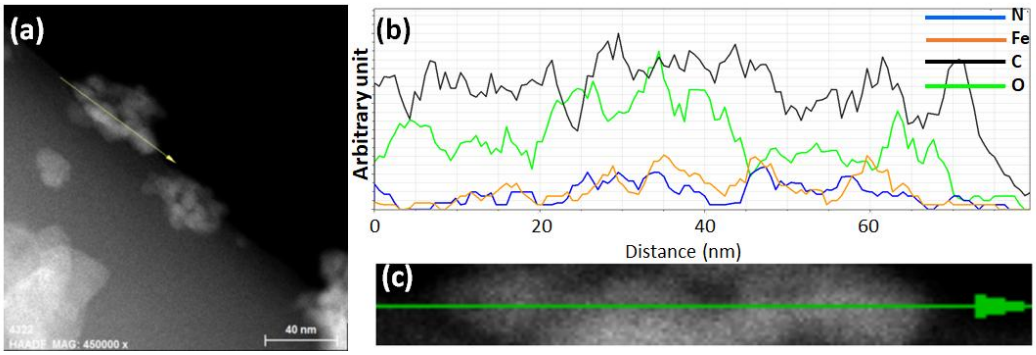

Figure 6. STEM-HAADF-EDS line scan analyses of Fe-Por functionalized graphene: (a) STEM-HAADF micrograph on the chosen area where a line scan along the direction indicated by the yellow arrow was performed. (b) Corresponding STEM-EDS line scan spectrum showing the variation of the Nitrogen (in blue), Iron (in orange), Carbon (in black) and Oxygen (in green) signal recorded along the scanning direction indicated by the green arrow in (c). (c) Zoom of the analyzed area indicated by the yellow arrow in (a).

X-ray Photoelectron Spectroscopy (XPS) technique has been used in order to corroborate the STEM-HAADF-EDS analyses and to characterize the chemical composition and state of elements present in the investigated nano-hybrid materials. Figure 7 displays the survey spectra of as-prepared nano-hybrids materials. It can be seen that only four peaks corresponding to Si2s, Si2p, C1s, and O1s elements were detected in the spectrum of graphene (Figure 7(a)), originated from SiO_2/Si substrate and graphene. However, after functionalization with Fe-Phc, two additional peaks can be observed, characteristic of Fe and

N, suggesting the successful grafting of phthalocyanines onto the graphene surface. Similar results were also obtained for Fe-Por-graphene and Co-Por-graphene presented in Figure S21, Figure S22, Table S2 and Table S3. After graphene functionalization with Fe-Phc, Fe and N elements are detected, and their content is 0.3% and 1.3%, respectively. Since graphene does not contain Fe and N but Fe-Phc does, it can be said that the Fe and N elements in Fe-Phc-graphene originate from Fe-Phc, indicating that Fe-Phc is physi-adsorbed on the surface of the graphene to form a nano-hybrid material. We note that the ratio of Fe and N is different from the expected theoretical one. this is due to the inevitable problem of surface contamination of CVD-graphene sheets. To detach the graphene layer from the Cu substrate wet etching using $FeCl_3$, solutions was performed.

Furthermore, to investigate the chemical states of elements, narrow scans were performed on the C1s, N1s, and F2p (Figure S23). To summarize at this point, the various results obtained by spectroscopic and microscopic techniques have demonstrated that there are π-π electron interactions and an effective charge transfer between porphyrins or phthalocyanines and graphene. These results suggest that the functionalization of graphene with different Por or Phc is a promising approach to develop new materials which could be used in a new generation of gas sensors.

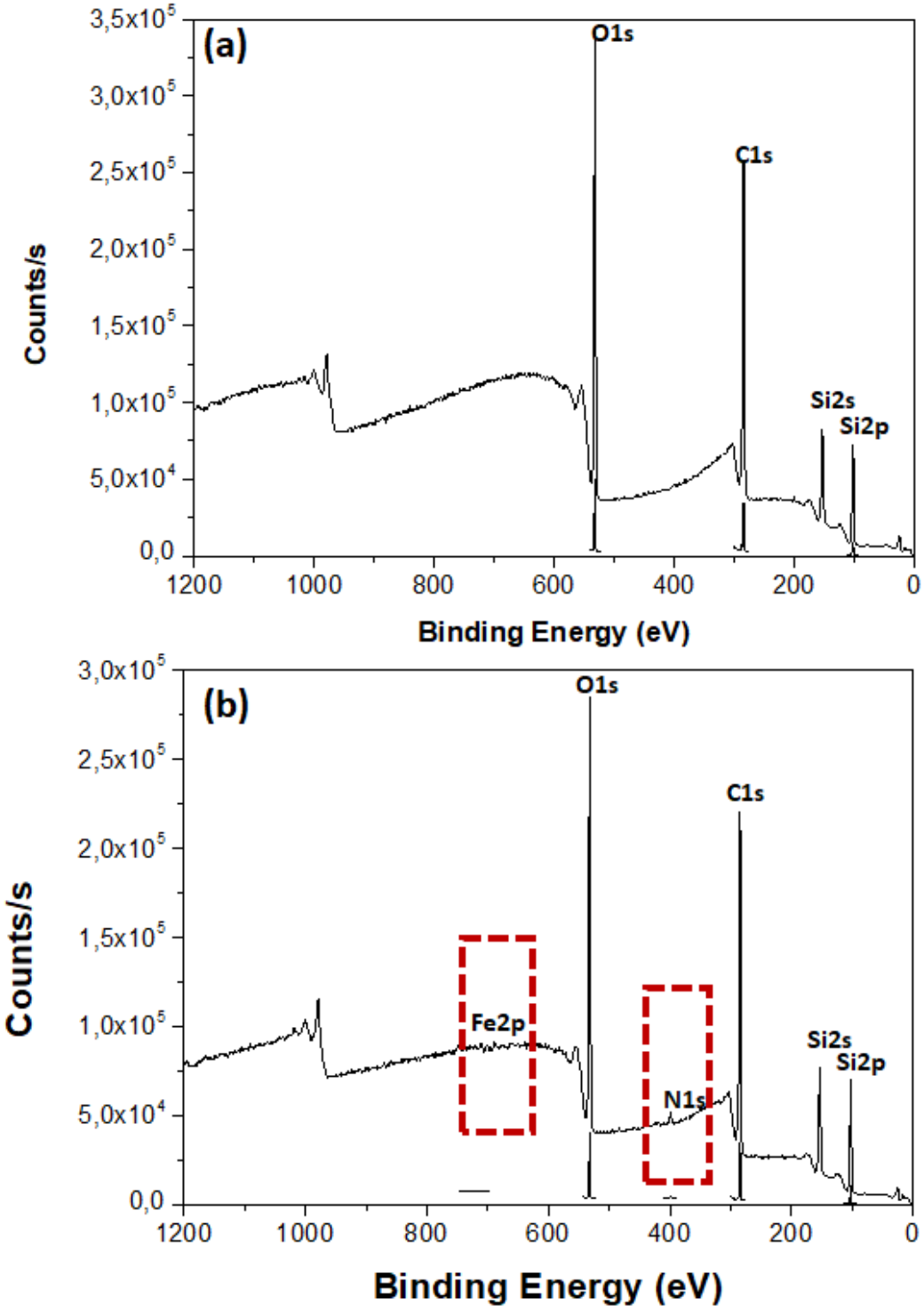

Figure 7. XPS spectra of pristine graphene and Fe-Phc-graphene.

To analyze the non-covalent doping graphene mechanism by Co-Por molecule, periodic unrestricted DFT calculations were carried out using CRYSTAL17 package [40]. The graphene has been widely studied and previous theoretical works indicate that PBE functional is widely used in graphene studies [41-43]. The calculated bond length of graphene equals to 1.429 Å which corresponds to lattice parameter a = 2.475 Å. This value is in agreement with the experimental value of 1.420 Å [44].

From geometriy optimizations of the global complex, the Co-Por molecule adsorbs on the graphene surface in a bridge site such that the the metal center (cobalt (II)) interacts with a C-C bond of graphene (see Figures 8(a) and 8(b)). The computed binding energy is E_b = -180.67 kJ.mol^{-1}. To the best of our knowledge, there is no former information in the literature to compare with this value, but Touzeau et al. reported a value of -151.04 kJ.mol^{-1} for the adsorption of Fe-Por on graphene [45].

The variation of Fermi levels with the addition of Co-Por molecule on the graphene surface is presented in Figure 8(c). The Fermi level, Ef, is increased with the functionalization of graphene surface, with Ef - Ef(graphene) = 0.1233 eV, indicating that Co-Por is electron donor. This result is confirmed by the net charge transfer (Δq) from Mulliken analysis giving Δq(graphene) = -0.0789475e after functionnalization, but also by the HOMO energy levels lying 0.076 eV above the graphene Fermi level before functionalization (see SI for details). Thus, the semimetal graphene is n-type doped by the functionalizing molecule. These results are in line with the experimental results.

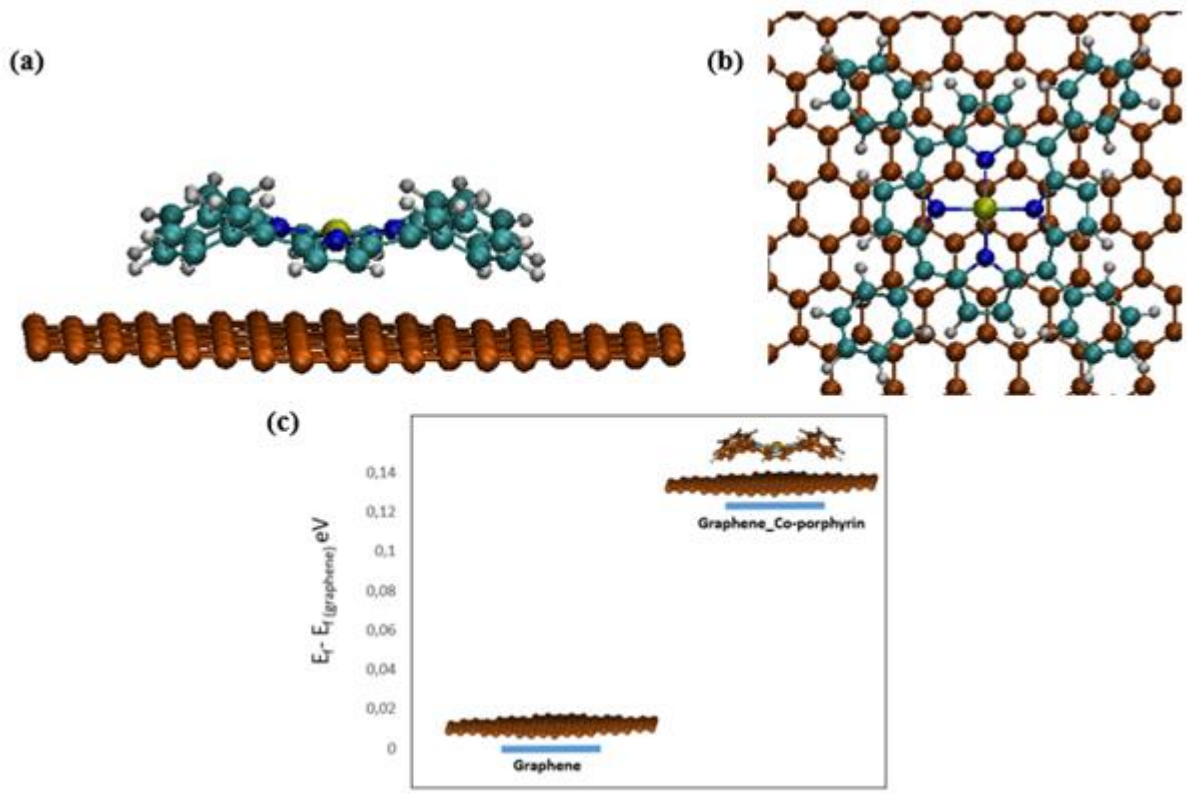

Figure 8. Optimized geometry of the Co-Por adsorbed on the graphene. (a) front view, (b) top view and (c) fermi levels of graphene pristine and graphene_Co-Por at the PBE-D3/6-31G** level of theory.

Electrical characterizations were performed to confirm on the one hand the successful formation of nano-hybrid materials, and on the other hand, to investigate the influence of the functionalization on the electronic properties of graphene. The charge transport studies were carried out using electrolyte-gated GFET devices under ambient conditions. This device architecture was chosen because GFETs show superior performance (i.e. increased transconductance: ($\Delta I_{DS}/\Delta V_{GS}$) when operated in electrolyte gated mode compared to the conventional back-gated devices owing to the few angstroms thick electric double layers formed between the electrolyte-semiconductor and electrolyte-reference electrode interfaces [46]. The inset of Figure 9(a) and Figure S25 shows a schematic illustration of an electrolyte gated field-effect transistor consisting of a graphene sheet as the channel, on top of a SiO_2/ Si substrate (a 200 nm thick SiO_2 film and a 725 µm thick doped Si (100) wafer), a gold electrode on the top of the SiO_2/Si substrate. A droplet of deionized water is used as the gate

dielectric. Figure S26 presents an SEM image of the GFET before functionalization. The measurements were carried out with a drain-source bias of 1 mV, and a gate voltage sweep from 0 to 1V in steps of 0.02 V. Figure 9(a) shows the current-voltage (I_{DS}-V_{GS}) curves of the graphene transistor before functionalization. The (I_{DS}-V_{GS}) curve of graphene shows the typical ambipolar character of GFET, i.e., the curve is symmetric around the minimum of I_{DS}, which is called V_{Dirac} or Dirac point (corresponding to the channel conductance minimum). It also shows that, due to the fabrication processing, our graphene is initially p-type doped with the Dirac point found at positive V_{GS} values. The transfer curve was repeated several times (5-10 times) to obtain a stable position before functionalization (see Figure 9(a)). To reveal the doping effect of various aromatic molecules, we examined the shift of the Dirac point, which is directly related to the Fermi energy change in the graphene. The I_{DS}-V_{GS} curves for functionalized graphene with Co-Por, Fe-Por, and Fe-Phc are presented in Figures 9(b), 9(c), and 9(d), respectively. In Figures 9(b) and 9(c), the Dirac point is downshifted, thus indicating that Co-Por and Fe-Por are causing n-type doping of graphene and suggest an electron transfer from these molecules to graphene. This behavior has been observed consistently in various devices prepared under the same conditions (see Figure S27 and S28 in supporting information). The work function difference between graphene and these compounds explains this behavior when the compounds are deposited on the graphene surface. The Fermi energy levels align by charge transfer from Co-Por or Fe-Por to graphene through the interface between them, inducing n-type doping [23, 47]. However, the transfer curves of functionalized graphene with Fe-Phc show a positive shift in the Dirac point (see Figure 9(d)), suggesting a hole doping of graphene. The statistical results confirm this behavior (Figure S29 in supporting information). The calculated electron and hole mobilities extracted from the transfer curve are summarized in (Table S5 in SI).

In electrolyte-gated graphene transistors, the geometric capacitance is set by the EDLs that form at graphene/electrolyte and gate electrode/electrolyte interfaces. This layer has a thickness equal to the Debye length, typically one to several nanometers, determining the (high) geometrical gate capacitance. Because of the vanishingly small graphene DOS near the Dirac point, the quantum capacitance is of the same order of magnitude as the geometrical capacitance in this case, and both need to be considered when extracting transistor parameters, such as the carrier mobility. However, direct measurement of the Debye length is not possible. A rough estimation using Debye–Hückel theory would be incorrect since the dielectric constant of water close to a hydrophobic surface like graphene is different (smaller) than in bulk. We, therefore, used a different approach that consists of fitting the transistor conductance data using a model that does not rely on the explicit knowledge of the geometric capacitance. The model describes the channel conductance as a function of the position of the Fermi level, based on carrier resonant scattering due to strong short-range potentials originating from impurities adsorbed at the graphene surface [48- 50] for a detailed discussion of the model and methodology.

Electrical characterizations evidence that the graphene is successfully functionalized with Por and Phc and a charge transfer between the compound molecules and graphene occurs, confirming the non-covalent functionalization of graphene. Therefore, it is concluded that the Co-Por and Fe-Por cause n-type doping while Fe-Phc imposes p-type doping on graphene. These results are in good agreement with earlier ones of graphene non-covalently functionalized with porphyrins and phthalocyanines [23, 47]. Finally, Raman and transport experiments converge on the charge transfer signal between graphene and the aromatic molecules.

The presence of Fe, Co, and N revealed by EDS and XPS analysis, the shift of G and 2D bands observed in Raman spectra, and the shift of the Dirac point after graphene

functionalization all indicate the successful non-covalent functionalization of graphene and the electron transfer process between the physi-adsorbed molecules and graphene. Therefore, Por and Phc can modulate the doping level or the Fermi energy of graphene.

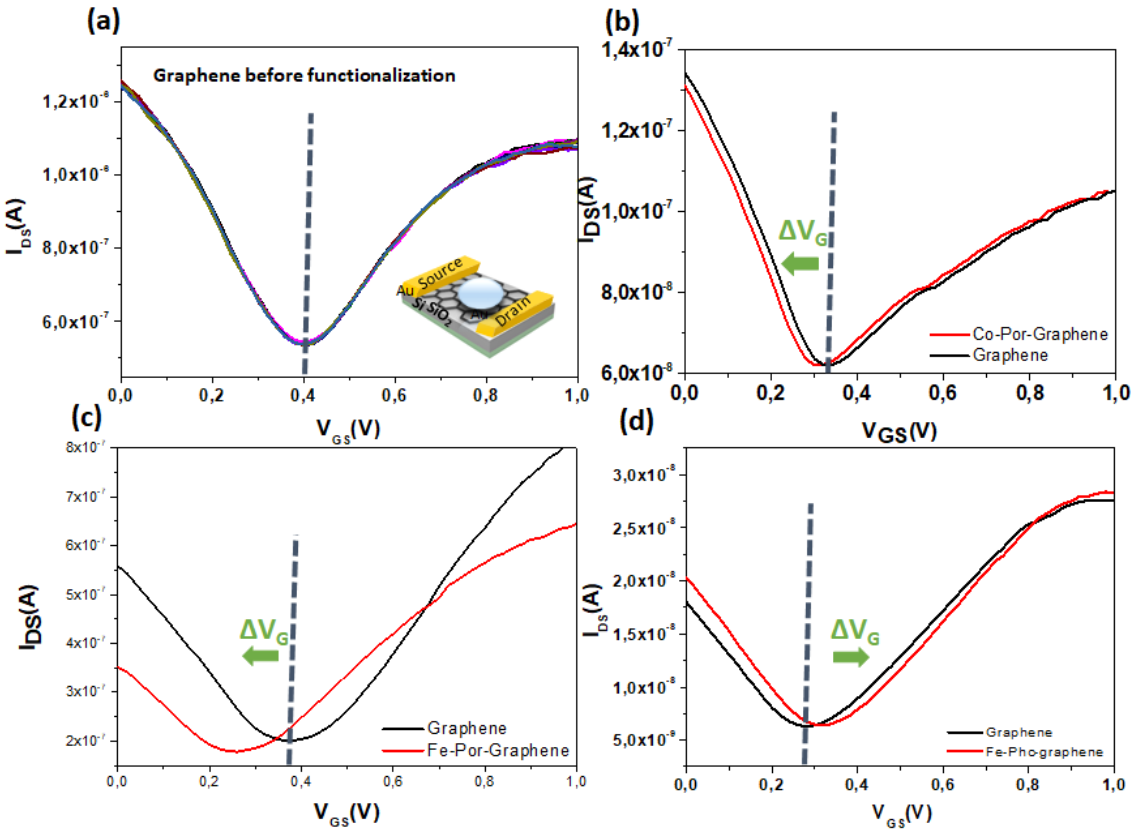

Figure 9. Transfer characteristics of graphene field-effect transistors before and after functionalization with Por and Phc. (a-d) Drain current vs. gate voltage characteristics of as-fabricated electrolyte-gated GFET(a) and functionalized GFET with Co-Por (b), Fe-Por (c), and (d) Fe-Phc. The Dirac point is shifted after functionalization in all cases. The dotted lines in (b-d) indicate the position of V_{Dirac} before functionalization.

4. Conclusion

Graphene nano-hybrid materials have been successfully prepared through a facile and straightforward process. The presence of Fe-Por, Co-Por, and Fe-Phc in the nano-hybrid materials was confirmed by EDS and XPS analysis. The non-covalent functionalization and the charge transfer between graphene and physi-adsorbed molecules were evidenced by Raman spectroscopy and electrical characterizations. SEM and TEM images evidenced the

morphologies of nano-hybrid materials. Considering the remarkable properties of graphene and MPo or MPc, these nano-hybrids materials might have potential applications in large-area electronics, such as sensors, solar cells, and nano-electronics. The application of these nanomaterials to explore their unique properties is underway in our group.

CRediT authorship contribution statement

F. Bouanis, A. Yassar, D. Pribat, J. Borme, P. Alpuim and C. Leonard planned and conceived the experiments and studies. C. M. Abreu, J. Borme and P. Alpuim synthesized the graphene and prepared electrolyte-gated GFETs. F.B. and M.D. prepared and characterized the surface by Raman Spectroscopy, AFM and SEM-EDX. F.B., M.D. and I. F. prepared and performed the HR-TEM-STEM studies. F.B, M.D. and C.J. prepared and performed XPS studies. F.B. and M.D. prepared the devices and performed the transport studies. C.L. and M.B. carried out the theoretical studies. All authors contributed to the analysis of the different studies. F.B. wrote the paper with contributions from all the authors.

Acknowledgments

F.Z.B and J.B acknowledge a grant from Hubert Curien – Fundação para a Ciência e a Tecnologia (FCT) Partnership (PHC-PESSOA 2D GAS SENS). Graphene field-effect transistors were provided through ASCENT+ collaboration from European Union's Horizon 2020 research and innovation programme, grant agreement 871130. In addition, FCT partially supported UMinho's research in the framework of the Strategic Funding UIDB/04650/2020. This work was carried out with partial support from LABEX MMCD. The authors acknowledge financial support from the French state managed by the National Research Agency under the Investments for the Future program under the references ANR-10-EQPX-50, pole NanoMAX and pole NanoTEM. Part of the TEM analysis was carried out at Centre Interdisciplinaire de Microscopie électronique de l'X (CIMEX), gratefully acknowledged. The authors acknowledge the help and the support from Dr. Simons Hallais for AFM analysis.

Declaration of Competing Interest

The authors declare that they have no known competing financial interests or personal relationships which have or could be perceived to have influenced the work reported in this article.

Supporting Information. Brief descriptions in nonsentence format listing the contents of the files supplied as Supporting Information.

References:

[1] D. Li, R. B. Kaner, Materials science. Graphene-based materials, Science 320 (2008) 1170. DOI: 10.1126/science.1158180.

[2] D.A. Dikin, S. Stankovich, E.J. Zimney, R.D. Piner, G.H.B. Dommett, G. Evmenenko, S. T. Nguyen, R.S. Ruoff, Preparation and characterization of graphene oxide paper, Nature 448 (2007) 457. DOI:10.1038/nature06016.

[3] J.S. Bunch, A.M. van der Zande, S.S. Verbridge, I.W. Frank, D.M. Tanenbaum, J.M. Parpia, H.G. Craighead, P.L. Mceuen, Electromechanical resonators from graphene sheets, Science 315 (2007) 490. DOI: 10.1126/science.1136836.

[4] A.K. Geim, K.S. Novoselov, The rise of graphene, Nat. Mater. 6 (2007) 183. DOI: 10.1038/nmat1849.

[5] X.C. Dong, D.L. Fu, W.J. Fang, Y.M. Shi, P. Chen, L.J. Li, Doping Single-Layer Graphene with Aromatic Molecules, Small 5 (2009) 1422. DOI: 10.1002/smll.200801711.

[6] Y.M. Shi, X.C. Dong, P. Chen, J.L. Wang, L.J. Li, Effective doping of single-layer graphene from underlying SiO_2 substrates, Phys. Rev. B 79 (2009) 115402. DOI: 10.1103/PhysRevB.79.115402.

[7] A. Das, S. Pisana, B. Chakraborty, S. Piscanec, S.K. Saha, U.V. Waghmare, K.S. Novoselov, H.R. Krishnamurthy, A.K. Geim, A.C. Ferrari, A.K. Sood, Monitoring dopants by Raman scattering in an electrochemically top-gated graphene transistor, Nat. Nanotechnol. 3 (2008) 210. DOI: 10.1038/nnano.2008.67.

[8] Y. Xu, Z. Liu, X. Zhang, Y. Wang, J. Tian, Y. Huang, Y. Ma, X. Zhang, Y. Chen, A Graphene Hybrid Material Covalently Functionalized with Porphyrin: Synthesis and Optical Limiting Property, Adv. Mater. 21 (2009) 1275–1279. DOI: 10.1002/adma.200801617.

[9] H. Yang, C. Shan, F. Li, D. Han, Q. Zhang, L. Niu, Covalent functionalization of polydisperse chemically-converted graphene sheets with amine-terminated ionic liquid, Chem. Commun. 26 (2009) 3880 – 3882. DOI: 10.1039/B905085J

[10] X. Zhang, Y. Feng, S. Tang, W. Feng, Preparation of a graphene oxide–phthalocyanine hybrid through strong π–π interactions, Carbon 48 (2010) 211–216. DOI: 10.1016/j.carbon.2009.09.007.

[11] Y. Xu, H. Bai, G. Lu, C. Li, G. Shi, Flexible Graphene Films via the Filtration of Water-Soluble Noncovalent Functionalized Graphene Sheets, J. Am. Chem. Soc. 130 (2008) 5856–5857. DOI: 10.1021/ja800745y

[12] Q. Su, S. Pang, V. Alijani, C. Li, X. Feng, K. Müllen, Composites of Graphene with Large Aromatic Molecules, Adv. Mater. 21 (2009) 3191 – 3195. DOI: 10.1002/adma.200803808.

[13] Y. Zhao, M. Gobbi, L. E. Hueso, P. Samorì, Molecular Approach to Engineer Two-Dimensional Devices for CMOS and beyond-CMOS Applications, Chem. Rev. (2021). DOI: 10.1021/acs.chemrev.1c00497

[14] R. Phillipson, C.J. Lockhart de la Rosa, J. Teyssandier, P. Walke, D. Waghray, Y. Fujita, J. Adisoejoso, K.S. Mali, I. Asselberghs, C. Huyghebaert, H. Uji-i, S. D. Gendt, S.D. Feyter, Tunable doping of graphene by using physisorbed self-assembled networks, Nanoscale 8 (2016) 20017-20026. DOI: 10.1039/C6NR07912A.

[15] C. Coletti, C. Riedl, D.S. Lee, B. Krauss, L. Patthey, K. von Klitzing, J.H. Smet, U. Starke, Charge neutrality and bandgap tuning of epitaxial graphene on SiC by molecular doping, Phys. Rev. B 81 (2010) 235401. DOI:10.1103/PhysRevB.81.235401.

[16] X.C. Dong, Y.M. Shi, Y. Zhao, D.M. Chen, J. Ye, Y.G. Yao, F. Gao, Z.H. Ni, T.Yu, Z.X. Shen, Y.X. Huang, P. Chen, L.J. Li, Symmetry Breaking of Graphene Monolayers by

Molecular Decoration, Phys. Rev. Lett. 102 (2009) 135501. DOI: 10.1103/PhysRevLett.102.135501

[17] S.J. Kim, W. Song, S. Kim, M-A Kang, S. Myung, S.S. Lee, J. Lim, K-S. An, Tunable functionalization of graphene nanosheets for graphene-organic hybrid photodetectors, Nanotechnology 27 (2016) 075709. DOI: 10.1088/0957-4484/27/7/075709

[18] Y. Lee, S.H. Yu, J. Jeon, H. Kim, J.Y. Lee, H. Kim, J-H. Ahn, E. Hwang, J.H. Cho, Hybrid structures of organic dye and graphene for ultrahigh gain photodetectors, Carbon 88 (2015) 165–72. DOI: 10.1016/j.carbon.2015.02.071

[19] C.G. Claessens, U. Hahn, T. Torres, Phthalocyanines: from outstanding electronic properties to emerging applications. Chem Rec 8 (2008) 75–97. DOI: 10.1002/tcr.20139.

[20] N. Alzate-Carvajal, A. Luican-Mayer, Functionalized Graphene Surfaces for Selective Gas Sensing, ACS Omega 5 (2020) 21320−21329. DOI: 10.1021/acsomega.0c02861

[21] Arramel , A. Castellanos-Gomez, B.J. Wees, Band Gap Opening of Graphene by Non-covalent π-π Interaction with Porphyrins, Graphene 2 (3) (2013) 102-108. DOI: 10.4236/graphene.2013.23015.

[22] A.S. Gajarushi, D. Pathan, T.R. Naik, M. Walawalkar, M. Ravikanth, A. Kottantharayil, V.R. Rao, Porphyrin Induced Changes in Charge Transport of Graphene FET, Proceedings of the 16th International Conference on Nanotechnology Sendai, Japan, August 22-25, 2016. http://b-dig.iie.org.mx/BibDig2/P16-0585/papers/0303.pdf

[23] C. Mackin, V. Schroeder, A. Zurutuza, C. Su, J. Kong, T.M. Swager, T. Palacios, Chemiresistive Graphene Sensors for Ammonia Detection, ACS Appl. Mater. Interfaces 10 (18) (2018) 16169–16176. DOI: 10.1021/acsami.8b00853

[24] S. Pyo , J. Choi, J. Kim, Improved photo- and chemical-responses of graphene via porphyrin-functionalization for flexible, transparent, and sensitive sensors, Nanotechnology 30 (21) (2019) 215501. DOI: 10.1088/1361-6528/ab048d.

[25] R. Campos, G. Machado Jr, M.F. Cerqueira, J. Borme, P. Alpuim, Wafer scale fabrication of graphene microelectrode arrays for the detection of DNA hybridization, Microelectron. Eng. 189 (2018) 85–90. DOI : 10.1016/j.mee.2017.12.015.

[26] F. Z. Bouanis, M. Bensifia, I. Florea, S. Mahouche chergui, B. Carbonnier, D. Grande, C. Léonard, A. Yassar, D. Pribat, Non-covalent functionalization of single walled carbon nanotubes with Fe-/Co-porphyrin and Co-phthalocyanine for field-effect transistor applications, Organic Electronics 96 (2021) 106212. DOI: 10.1016/j.orgel.2021.106212

[27] J.W. Suk, A. Kitt, C.W. Magnuson, Y. Hao, S. Ahmed, J. An, A.K. Swan, B.B. Goldberg, R.S. Ruoff, Transfer of CVD-Grown Monolayer Graphene onto Arbitrary Substrates, ACS Nano 5 (9) (2011) 6916–6924. DOI: 10.1021/nn201207c.

[28] D.A. Shirley, High-Resolution X-Ray Photoemission Spectrum of the Valence Bands of Gold. Phys. Rev. B 5 (1972) 4709–4714. DOI: 10.1103/PhysRevB.5.4709.

[29] P.D. Cabral, T. Domingues, G. Machado Jr., A. Chicharo, F. Cerqueira, E. Fernandes, E. Athayde, P. Alpuim, J. Borme, Clean-Room Lithographical Processes for the Fabrication of Graphene Biosensors, Materials 13 (2020) 5728. DOI: 10.3390/ma13245728.

[30] S. De, P. J. King, M. Lotya, A. O'Neill, E. M. Doherty, Y. Hernandez, G. S. Duesberg, J. N. Coleman, Flexible, transparent, conducting films of randomly stacked graphene from surfactant-stabilized, oxide-free graphene dispersions, Small 6 (2010) 458 – 464. DOI: 10.1002/smll.200901162

[31] C. Casiraghi, A. Hartschuh, H. Qian, S. Piscanec, C. Georgi, A. Fasoli, K.S. Novoselov, D.M. Basko, A.C. Ferrari, Raman spectroscopy of graphene edges, Nano Lett. 9 (2009) 1433. DOI: 10.1021/nl8032697

[32] R. Voggu, B. Das, C.S. Rout, C.N. R. Rao, Effects of Charge Transfer Interaction of Graphene with Electron Donor and Acceptor Molecules Examined Using Raman Spectroscopy and Cognate Techniques. J. Phys.: Condens. Matter 20 (2008) 472204. DOI:10.1088/0953-8984/20/47/472204

[33] T. Sagara, M. Fukuda, N. Nakashima, Electroreflectance Study of Hemin Adsorbed on a HOPG Electrode: Estimation of Molecular Orientation and Analysis of Nonfaradaic Electroreflectance Signal Due to the Stark Effect, J. Phys. Chem. B 102 (1998) 521-527. DOI: 10.1021/jp9713928

[34] M.V.O. Moutinho, A. Lombardo, T.S. Kulmala, A.C. Ferrari, Quantifying defects in graphene via Raman spectroscopy at different excitation energies, Nano Lett. 11 (2011) 3190–3196. DOI: 10.1021/nl201432g.

[35] A.C. Ferrari, J.C. Meyer, V. Scardaci, C. Casiraghi, M. Lazzeri, F. Mauri, S. Piscanec, D. Jiang, K.S. Novoselov, S. Roth, A.K. Geim, Raman Spectrum of Graphene and Graphene Layers, Phys. Rev. Lett. 97 (2006) 187401. DOI: 10.1103/PhysRevLett.97.187401.

[36] C. Faugeras, A. Nerriere, M. Potemski, A. Mahmood, E. Dujardin, C. Berger, W.A. de Heer, Few-layer graphene on SiC, pyrolitic graphite, and graphene: A Raman scattering study, Appl. Phys. Lett. 92 (2008) 011914. DOI: 10.1063/1.2828975

[37] X. Dong, Y. Shi, P. Chen, Q. Ling, W. Huang, Aromatic Molecules Doping in Single-Layer Graphene Probed by Raman Spectroscopy and Electrostatic Force Microscopy. Jpn. J. Appl. Phys. 49 (1) AH04 (2010). DOI: 10.1143/JJAP.49.01AH04

[38] G. Wu, X. Tang, M. Meyyappan, K.W.C. Lai, Doping effects of surface functionalization on graphene with aromatic molecule and organic solvents. Applied Surface Science 425 (2017) 713–721.DOI: 10.1016/j.apsusc.2017.07.048

~~[39] D. Yang, A. Velamakanni, G. Bozoklu, S. Park, M. Stoller, R.D. Piner, S. Stankovich, I. Jung, D.A. Field, C.A. Ventrice, Chemical analysis of graphene oxide films after heat and chemical treatments by X-ray photoelectron and Micro-Raman spectroscopy, Carbon 47 (2009) 145–152. https://doi.org/10.1016/j.carbon.2008.09.045~~

[39] S. Pratontep, M. Brinkmann, F. Nüesch, L. Zuppiroli, Correlated growth in ultrathin pentacene films on silicon oxide: Effect of deposition rate, Phys. Rev. B 69 (2004) 165201. DOI:https://doi.org/10.1103/PhysRevB.69.165201

[40] R. Dovesi, A. Erba, R. Orlando, C.M. Zicovich-Wilson, B. Civalleri, L. Maschio, M. Rérat, S. Casassa, J. Baima, S. Salustro, B. Kirtman, Quantum-mechanical condensed matter simulations with CRYSTAL, WIREs Comput. Mol. Sci., 8 (4) (2018) e1360. DOI: 10.1002/wcms.1360

[41] J. Dai, J. Yuan, P. Giannozzi, Gas adsorption on graphene doped with B, N, Al, and S: A theoretical study, Appl. Phys. Lett., 95(23) (2009) 232105. DOI: 10.1063/1.3272008.

[42] K. Suggs, D. Reuven, X. Q. Wang, Electronic properties of cycloaddition-functionalized graphene, J. Phys. Chem. C 115(8) (2011) 3313–3317. DOI: 10.1021/jp111637b.

[43] Y. Duan, C.D. Stinespring, B. Chorpening, Electronic Structures, Bonding Configurations, and Band-Gap-Opening Properties of Graphene Binding with Low-Concentration Fluorine, Chemistry Open 4(5) (2015) 642-650. DOI: 10.1002/open.201500074.

[44] Y. Baskin, L. Meyer, Lattice constants of graphite at low temperatures, Phys. Rev., 100 (2) 1955. DOI: 10.1103/PhysRev.100.544.

[45] J. Touzeau, F. Barbault, F. Maurel, M. Seydou, Insights on porphyrin-functionalized graphene: theoretical study of substituent and metal-center effects on adsorption, Chem. Phys. Lett. 713 (2018) 172-179. DOI: 10.1016/j.cplett.2018.10.046

[46] F. Torricelli, D.Z. Adrahtas, Z. Bao, M. Berggren, F. Biscarini, A. Bonfiglio, C.A. Bortolotti, C.D. Frisbie , E. Macchia, G.G. Malliaras, I. McCulloch, M. Moser, T.Q. Nguyen, R.M. Owens, A. Salleo, A. Spanu, L. Torsi, Electrolyte-gated transistors for enhanced performance bioelectronics. 66 (2021). DOI: 10.1038/s43586-021-00065-8

[47] P.H. Ho, S.S. Li, Y.T. Liou, C.Y. Wen, Y.H. Chung, C.W. Chen, Wavelength-selective dual p- and n-type carrier transport of an organic/graphene/inorganic heterostructure, Adv. Mater. 27 (2015) 282–7. DOI: 10.1002/adma.201403694.

[48] N.C.S. Vieira, J. Borme, G. Machado Jr, F. Cerqueira, P. P. Freitas, V. Zucolotto, N. M. R. Peres, P. Alpuim, Graphene field-effect transistor array with integrated electrolytic gates scaled to 200 mm, J. Phys.: Condens. Matter 28 (2016) 085302. DOI:10.1088/0953-8984/28/8/085302

[49] A. Ferreira, J. Viana-Gomes, J. Nilsson, E.R. Mucciolo, N.M.R. Peres, A.H. Castro Neto, Unified description of the dc conductivity of monolayer and bilayer graphene at finite densities based on resonant scatterers, Physical review B 83 (2011) 165402. DOI: 10.1103/PhysRevB.83.165402

[50] N. M. R. Peres, *Colloquium*: The transport properties of graphene: An introduction, Rev. Mod. Phys. 82 (2010) 2673. DOI:10.1103/RevModPhys.82.2673